Received April 19, 2018, accepted May 12, 2018, date of publication May 17, 2018, date of current version August 28, 2018.

Digital Object Identifier 10.1109/ACCESS.2018.2837652

Multi-Objective Optimization Discharge Method for Heating Lithium-Ion Battery at Low Temperatures

JIUYU DU[1], ZHE CHEN[1,2], and FEIQIANG LI[1,3]

[1]State Key Laboratory of Automotive Safety and Energy, Tsinghua University, Beijing 100084, China
[2]College of Electrical and Electronics Engineering, Harbin University of Science and Technology, Harbin 150080, China
[3]Zhengzhou Yutong Bus Co., Ltd, Zhengzhou 450061, China

Corresponding author: Jiuyu Du (dujiuyu@tsinghua.edu.cn)

This work was supported by the National Key Technologies R&D Program of MOST under Grant 2016YFB0101801.

ABSTRACT Lithium battery for electric vehicle exhibits poor performance in durability and discharging efficiency under cold environment, therefore the traction battery must be heated to some suitable operation temperature before charging process begins. Self-heating by discharging current of the battery is recognized as a high-efficient and cost-effective method. However, the discharging current affects both the capacity degradation rate and heating time for lithium-ion battery greatly charged at low temperatures. Therefore, the discharging strategy should be optimized based on the parameters of the battery capacity fade rate and heating time, and it's the motivation of this research. The parameters of the Thevenin equivalent circuit model are set up and the temperature-rise model is identified by test data. To determine the optimal battery discharging current for heating, the dynamic programming algorithm is adopted The capacity fade rate and heating time is analyzed by setting different weighting factors in the heating process of battery temperatures rising from −10°C to +5°C. Compared with constant current discharging method, the multi-objective optimization self-heating method can decrease the battery capacity fade by 5.65%, the heating time is by 1.82%, and the power consumption by 3.04%. Therefore, it can be concluded that the proposed multi-objective optimization can optimize heating time and energy consumption at same time, with minimize capacity degradation.

INDEX TERMS Lithium-ion battery, battery equivalent circuit model, temperature-rise model, self-heating method, dynamic programming algorithm.

I. INTRODUCTION

Lithium batteries have become the main energy storage system for electric vehicles (EVs)due to their long cycle life, high energy density and excellent power performance [1]. However, the characteristics of lithium-ion batteries are affected by ambient temperature significantly [2]. As the temperature decreases, the internal resistance increases during the process of charging and discharging [3]. At low temperatures (for lithium ion phosphate (LFP) battery, it is ordinary below 0 °C, and for LiNiMnCoO2 (NCM) battery it is below −10 °C), the all-electric range(AER) of EVs declines greatly [4], making permanently damage on battery [5]. It is caused by decreases in electrolyte conductivity [6] and reaction kinetics [7], as well as the slowdown of diffusion rate for lithium ions in the cathode [8] under low temperatures. So far, it has been difficult to solve the problem of poor low-temperature performance of lithium batteries by innovations in battery materials [9]. Therefore, it is usually necessary to heat the battery to a suitable temperature before operating at low temperatures.

The heating method can be classified into three categories by heating source, including external heating, internal heating and a combination of internal and external heating. Song *et al.* [10] heated batteries by air convection, i.e., by heating the air-duct of the battery pack. The energy efficiency is low for this method due to its unnecessary energy loss during the heating process. Zhu *et al.* [11] established a warm-up management strategy based on the electric and thermal performance analysis and aging model of LFP batteries, which aimed at reducing the operating cost of EVs. The battery is heated from −10°C to 2°C by liquid heating, and the operating cost per cycle of the EV is reduced by

$50 compared to the case of the non-preheated condition. However, the method of heating by liquid causes a temperature gradient within the battery, adversely affecting the consistency of the battery pack. Zhang *et al.* [12] heated the battery using a broadband metal film that was powered by an external power source. Heated batteries can release 50% of the rated capacity compared with the case when batteries cannot be discharged without heating. Murashko *et al.* [13] used a plate heat exchanger for the heat transfer in battery pack thermal management system. The broadband metal film does not affect the cooling of the battery and has good thermal insulation properties, but EVs are powered by a plurality of cells through a series of parallel-connected battery packs [14]. The cells are closely arranged together. When the method of external heating is applied, the uneven heating of the individual cells will cause the local temperature of the battery pack to rapidly increase. The consistency of the battery pack will deteriorate, and the cycle life will be greatly shortened. In severe cases, it will cause thermal runaway, resulting in more serious accidents. Therefore, compared with the external heating method, the main advantage of the internal heating method is high energy efficiency and the ability to achieve uniform heating of the battery because of the heat generated by resistance during charge and discharge. Ji and Wang [15] divided battery packs into two groups for simulation. After the DC/DC boost, the two groups of batteries were alternately charged and discharged at a certain frequency to heat the batteries, obtaining an ideal temperature rise effect in the end. However, the heating process causes a current that is too large, and the battery charge voltage is significantly higher than the charge cut-off voltage, increasing the possibility of lithium dendrites. Zhang *et al.* [16] established a frequency-domain model for 3.1 Ah lithium-ion batteries and proposed to use sinusoidal alternating current to internally heat the batteries. However, the heating process has been accompanied by the problem of a high transient voltage, with a maximum recorded battery voltage in experiments of 4.5 V. In practical applications, if the amplitude and frequency of the alternating current (AC) are not properly selected, the battery may be over-voltage, causing some damage to the battery. Mohany *et al.* [17] exploited the increased internal resistance of battery to improve the capability and the current is shaped as bi-directional pulses to minimize total energy discharge. Zhao *et al.* [18] proposed to use a large current pulse to heat LFP batteries with a rated capacity of 12 Ah. The battery is heated from $-10°C$ to $3°C$ by 18 charge and discharge cycles, and the charge and discharge cut-off voltages are set as 2.1 V and 3.6 V, respectively. However, when this method is applied, the battery will often be charged at a high rate at low temperatures, thus causing serious damage to the battery. Ruan *et al.* [19] heated a battery from $-15°C$ to $+5.6°C$ within 338 seconds via a high-frequency alternating current, with a constant polarization voltage set as the boundary condition. However, the experiment only proved that the battery had no obvious capacity fade after heating 30 times at low temperatures and could not guarantee a good battery state of health after 30 heating cycles. Zhang *et al.* [20] internally heated a battery by inserting a nickel foil heating element inside a lithium-ion battery, which can raise the battery temperature from $-20°C$ to $0°C$ in 12.5 s with a power consumption of 2.9% of its rated capacity. However, the method requires a complex manufacturing process and a high production cost, which will not be easily accepted. The heating method that combines internal heating with external heating is more effective than a single form of heating. Sun [21] did not rely on an external power source to heat batteries, resulting in a small discharge rate of the battery supply energy to the electric film by using the heat generated by resistances. When the ambient temperature was $-17°C$, the battery temperature reached $8°C$, and the discharge energy increased by 0.36031-fold compared to the unheated battery. Jaguemont *et al.* [7] presents an electrical and thermal model of an lithium-ion battery pack to evaluating the losses under low temperature. Wang *et al.* [22] developed all-climate battery (ACB) using a new cell structure with an internal heating element. By the method, the ACB cell withstands more than 500 fast-charge cycles while the conventional cell incurs 20% capacity loss after only 12 cycles. This kind of heating method is of high efficiency and less degradation, however it is very challenging to change the battery structure and production process. Zhang *et al.* [23] also used a combination of internal and external methods to heat batteries using a positive temperature coefficient (PTC) heater supplied by the batteries. The PTC heater, which is located among the single cells in the battery pack, enables battery temperature increases from $-20°C$ to $-2°C$ within 3000 seconds, and the power consumption is 13% of the rated capacity. However, the combination of internal and external heating increases the complexity of design and the manufacturing cost of the battery pack design.

When the battery is discharged at low temperatures or high rates, the lithium ion potential embedded in the negative electrode is low, which easily causes lithium ions to be plated on the negative electrode surface in the form of metal and cannot be embedded in the negative electrode lattice. The lithium ions attached to the negative electrode surface gradually form lithium dendrites and eventually pierce the diaphragm, causing an internal short circuit [24]. Therefore, battery aging will depend on whether battery continuous charge current or pulse charging current is applied at low temperatures [25].

By the literatures above mentioned, it can be concluded that the effective low temperature heating method is a hot issue in the world, however, few studies have investigated the optimal charging method under low temperature, taking depreciation rate and the heating time as parameters.

The LFP batteries are chose as object. Based on the Thevenin equivalent circuit model, battery temperature-rise model and battery aging model, the heat generated by resistance at low temperatures is used for the internal battery heating. The model parameters affected by the battery temperature and State of Charge (SOC), therefore the optimal discharge current was solved by the dynamic

programming(DP) algorithm, which set the heating time and the capacity fade as the optimization objectives and the polarization voltage as the state variable.

Additionally, the influence of different weighting factors on the optimization result is discussed.

II. LITHIUM-ION BATTERY MODEL AND PARAMETER ACQUISITION

A. EXPERIMENTAL MATERIALS AND EQUIPMENT PLATFORM

A 32650 LFP battery is the testing object, and the basic parameters of the battery are shown in Table 1.

TABLE 1. Battery parameters.

Parameters	Symbol	Value
Mass	m	145 g
Surface area	A	8.641×10^{-3} m^2
Capacity	Q	5A·h
Voltage	V_{rate}	3.2 V
Upper cut-off voltage	V_{up}	3.65 V
Lower cut-off voltage	V_{low}	2.5 V

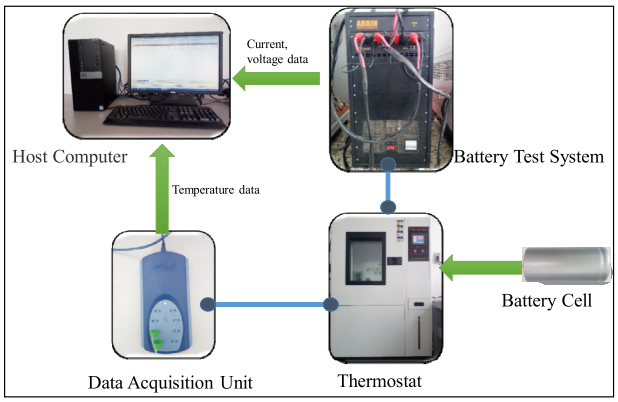

FIGURE 1. Test platform for battery.

The experimental platform is shown as Figure 1. The temperature sensor is placed in the middle of the battery, and the insulating film covers the entire side of the battery. The data collected by the temperature sensor are transmitted to the computer through the temperature measuring device, and the battery test system is controlled by the computer. The related equipment parameters are shown in Table 2.

B. BATTERY EQUIVALENT CIRCUIT MODEL AND PARAMETER IDENTIFICATION

The Thevenin equivalent circuit model can simulate the real electrical performance of the lithium battery [26], therefore is adopted to simulate the battery discharge process, shown in Figure 2. $R_r$is the ohmic internal resistance, U_r is the voltage at both ends of R_r, C_p and R_p, respectively, represent the polarization capacitance and the polarization resistance, U_p is the polarization voltage, R_{total} is the battery internal resistance, U_{OCV} is the open circuit voltage(OCV), E is the

TABLE 2. Equipment parameters.

Battery test system	Voltage range: 0 V~5 V Current range: 0 A~50 A Voltage accuracy: full-range ±0.05% FSR Current accuracy: full-range ±0.01% FSR Number of testing channels: 4
Thermal chamber	Temperature range: -50 °C ~+150 °C Temperature error: ≤ 0.5 °C Chamber volume: 0.5 m × 0.5 m × 0.6 m
Thermocouple temperature recorder	Number of testing channels: 4 Measuring temperature range：-270□～1820□ Interface method: USB

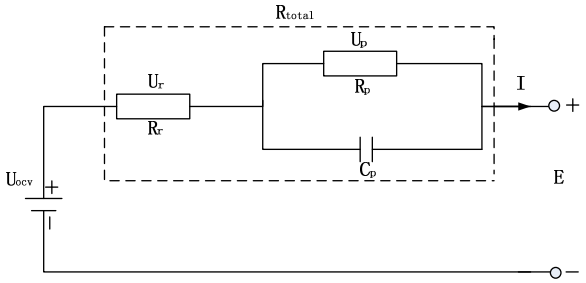

FIGURE 2. Thevenin equivalent circuit model.

terminal voltage, and I is the discharge current. The circuit mathematical model is described in equation (1).

$$\begin{cases} \dot{U}_p = -\dfrac{U_p}{R_p C_p} + \dfrac{I}{C_p} \\ E = U_{OCV} - U_p - IR_r \end{cases} \tag{1}$$

Referring to the experimental procedure for measuring the OCV of the battery in [27], the OCV is obtained at every 10% SOC at different temperatures in the range of −10°C to 25°C, as shown in Figure 3. The OCV of the battery

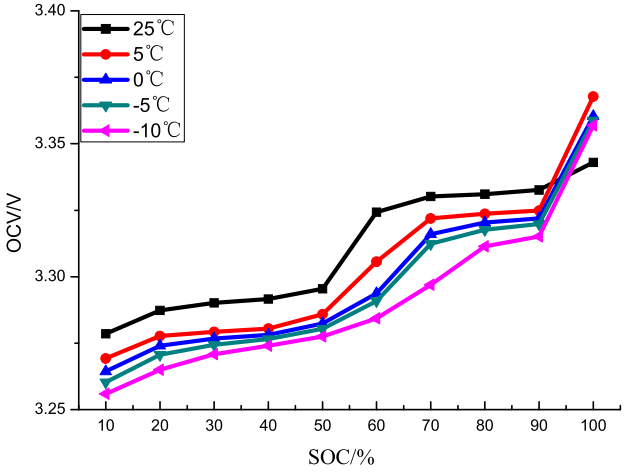

FIGURE 3. Battery OCV curves at different temperatures.

gradually increases with the increase of SOC. Under the SOC range of 10% ∼ 50%, the OCV of the battery slowly increases with the increase of SOC. When the SOC is greater than 50%, the increase rate of the OCV of the battery increases significantly. In the process of SOC increased from 90% to 100%, the OCV of battery is correspondingly increased to 40 mV. However, the OCV will be gradually decreased with the temperature decreasing, and the drop rate is approximately 0.6 mV/°C. Therefore, it can be seen that the influence of battery SOC on the OCV is significantly greater than that of ambient temperature.

To obtain the parameters for battery model at different temperatures and SOCs, the charging and discharging tests are performed, taking the hybrid pulse power characteristics (HPPC) test process as reference. The large charging and discharge rate will lead to significant heat generation, therefore, the charging and discharge rate in our tests are set as 0.75C and 1C respectively. The accuracy of the parameters is equivalent. The parameters for battery model are identified by a combination of excitation response analysis and the least squares method.

The recursive least square method [28] is an effective solution for parameter estimation. Based on the parameters estimation and the Thevenin equivalent circuit model, the mathematical model of the battery can be established as shown in equation (2):

$$E(s) = U_{OCV}(s) - \left(\frac{R_p}{R_p C_p s + 1} + R_r\right) I(s) \tag{2}$$

The output of the observation is y (s) $= U_{OCV}$ $(s) - E(s)$, the input is I(s), and the model transfer function is

$$Y(s) = \frac{R_r R_p C_p s + (R_r + R_P)}{R_p C_p s + 1} U(s) \tag{3}$$

The sampling period T $=$ 1 s, and equation (3) is transformed into a differential equation as shown in equation (4):

$$\begin{aligned} &U_{OCV}(k) - E(k) \\ &= \frac{R_p C_p}{R_p C_p + T}[U_{OCV}(k-1) - E(k-1)] \\ &\quad + \frac{R_r R_p C_p + R_p + R_r}{R_p C_p + T} I(k) - \frac{R_r R_p C_p}{R_p C_p + T} I(k-1) \end{aligned} \tag{4}$$

By substituting the current pulse and the voltage response at each SOC at different temperatures into equation (4), the battery model parameters are identified, and the results are shown in Figure 4.

From Figure 4 a), it can be seen that the ohmic resistance of the selected battery at a certain temperature is basically constant over the whole SOC range. The ohmic resistance at environmental temperature is approximately 0.01 Ω. The ohmic resistance gradually increases as temperature decreases. The ohmic resistance increases by approximately 10 mV if the temperature increases 5°C. All abovementioned indicate that ohmic resistance is mainly affected by environmental temperature, not SOC.

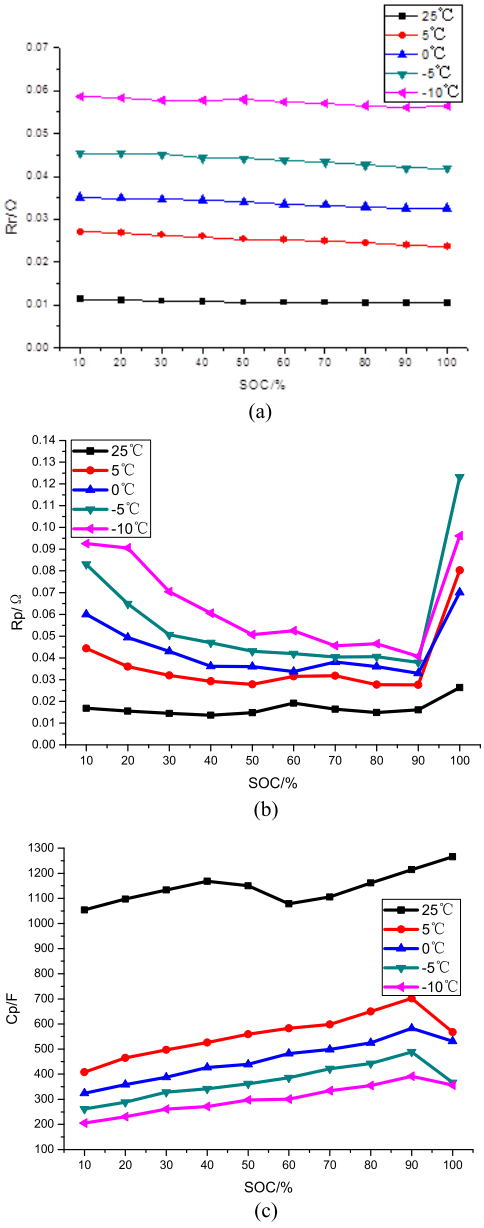

FIGURE 4. Parameter identification results at different temperature conditions and SOCs. (a) Identification of ohmic resistance. (b) Identification of polarization resistance. (c) Identification of polarization capacitance.

According to Figure 4 b), the polarization resistance of the selected battery changes as SOC changes at a certain temperature. At both ends of the battery SOC, the battery internal resistance changes more rapidly, and the resistance value is greater. When the battery is in the middle range of SOC, the polarization resistance changes relatively smoothly, and the resistance value is lower. In addition, the battery polarization resistance is also affected by ambient temperature; the polarization resistance increases approximately 7 mV when the ambient temperature decreases by 5°C.

Figure 4 c) shows that the polarization capacitance has a wave-like rise tendency as SOC increases at room temperature. When the battery temperature is from −10°C∼+5°C,

the trend of the polarization capacitance across the entire SOC range is basically the same. As the SOC increases from 10% to 90%, the polarization resistance gradually increases and reaches a maximum at 90% SOC. The polarization capacitance decreases with the increase in the SOC. In addition, the polarization capacitance is greatly affected by ambient temperature; the polarization capacitance decreases 0.008 F when the ambient temperature decreases by 5°C.

To sum up, the internal parameters of the battery equivalent model are mainly affected by the battery SOC and ambient temperature, so changes in battery SOC and temperature should be considered when the battery equivalent model is established.

In previous section, the battery model is set up by using MATLAB/ Simulink and The parameters for the simulation model are obtain by abovementioned methods. In order to verify the accuracy of battery parameters, the current obtained by dynamic stress test (DST) are put into the battery simulation model. Furthermore, the output voltage results are compared between that of the battery model and tests as shown in Figure 5. The maximum error is no more than 0.05V shown as Figure 6.

C. ESTABLISHMENT AND VERIFICATION OF THE BATTERY TEMPERATURE-RISE MODEL

The heat generated by the battery can be classified as irreversible heat and reversible heat. Irreversible heat includes

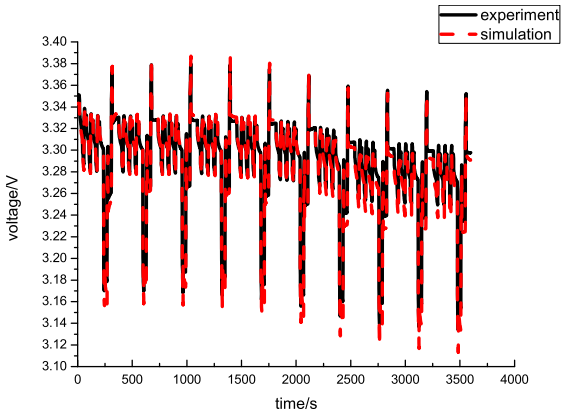

FIGURE 5. The comparison of terminal voltage between simulation and experimental values.

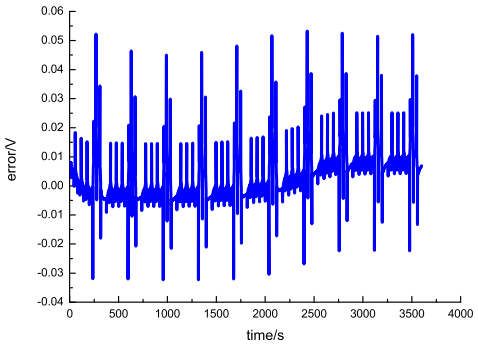

FIGURE 6. The voltage error between experimental and simulation results.

Joule heat and concentration polarization heat. Reversible heat is also called reaction heat, which is the energy released or absorbed by the electrochemical reaction in order to maintain the energy balance of the whole reaction. As described in [29], the battery heat model selected in this paper is shown as equation (5):

$$Q_t = Q_J + Q_r = I(E - U_{OCV}) + IT\frac{\partial U_{OCV}}{\partial T} \tag{5}$$

The direction of current is positive when charging and negative when discharging. E is the terminal voltage of the battery during charging and discharging, U_{OCV} is the OCV of the battery, Q_t is the total heat production power during charging and discharging, Q_J is the heat production power of irreversible heat, and Q_r represents the reaction heat, which depends on the battery charge and discharge currents and the effective entropy potential. The entropy potential is greatly affected by the battery SOC and varies with different chemical compositions [30]. During the charging and discharging of the battery, a voltage drop is generated at both ends of the internal resistance when the current flows through the internal resistance of the battery, and it is the main reason for the difference between the battery terminal voltage and the OCV [31].

$$Q_J = I(E - U_{OCV}) = I^2R_r + I_p^2R_p \tag{6}$$

The temperature rise of the lithium-ion battery is effected by the heat production, heat conduction and thermal diffusion [32]. When the battery is working at low temperatures, it not only produces heat but also generates heat radiation and convection to the outside, dissipating a portion of the heat, where the amount of heat dissipated by thermal radiation is negligible relative to the amount of heat dissipated by thermal convection. The dissipated power when the battery is in thermal convection with the external environment can be expressed by equation (7):

$$Q_{dis} = -hA(T - T_\infty) \tag{7}$$

Where, h is the equivalent heat transfer coefficient, A is the battery surface area, T is the battery temperature, and T_∞ is the ambient temperature.

In summary, the heat balance equation for the battery in the heating process is

$$\begin{aligned} mc\frac{dT}{dt} &= Q_J + Q_r + Q_{dis} \\ &= I^2R_r + I_p^2R_p + IT\frac{\partial U_{OCV}}{\partial T} - hA(T - T_\infty) \end{aligned} \tag{8}$$

Where, m is the battery mass, and c is the battery heat capacity. As equation (5) shows, the battery's total rate of heat generation is effected by the current, resistance, entropy potential, equivalent heat transfer coefficient and battery temperature. Therefore, the greater the current and the resistance are, the greater the battery heat rate; the higher the equivalent transfer coefficient and the battery temperature are, the greater the heat dissipation of the battery and the smaller the

total heating rate of the battery. The battery temperature-rise model is established considering the change of battery internal resistance and entropy coefficient caused by the change of battery temperature and SOC in the process of battery heating to ensure the accuracy of the temperature-rise model.

According to equation (8), we can obtain a linear differential equation for the battery temperature, as shown in equation (9):

$$\frac{dT(t)}{dt} = (\frac{I\frac{\partial V_{OCV}}{\partial T}}{mc} - \frac{hA}{mc})T(t) + \frac{I^2R_r}{mc} + \frac{I_p^2R_p}{mc} + \frac{hAT_\infty}{mc} \quad (9)$$

The continuous time system of equation (9) is discretized. Laplace transformation is applied in a sampling period to the left and right sides of equation (9); the original equation can be expressed as

$$sT(s) - T(t_0) = (\frac{I\frac{\partial V_{OCV}}{\partial T}}{mc} - \frac{hA}{mc})T(s) + (\frac{I^2R_r}{mc} + \frac{I_p^2R_p}{mc} + \frac{hAT_\infty}{mc})\frac{1}{s} \quad (10)$$

In equation (10), t_0 is the initial moment and t is the current moment. Under periodic sampling conditions, $t_0 = kT_0$, $t_0 = (k+1)T_0$, k $= 0, 1, 2, 3\cdots$; Then, equation (10) can be rewritten as

$$sT(s) - T(kT_0) = (\frac{I\frac{\partial V_{OCV}}{\partial T}}{mc} - \frac{hA}{mc})T(s) + (\frac{I^2R_r}{mc} + \frac{I_p^2R_p}{mc} + \frac{hAT_\infty}{mc})\frac{1}{s} \quad (11)$$

Rearranging equation (11), we derive

$$T(s) = \frac{T(kT_0)}{s + \frac{hA - I\frac{\partial V_{OCV}}{\partial T}}{mc}} + \frac{1}{s(s + \frac{hA - I\frac{\partial V_{OCV}}{\partial T}}{mc})} \cdot (\frac{I^2R_r + hAT_\infty}{mc} + \frac{I_p^2R_p}{mc}) \quad (12)$$

Laplace inverse transformation of equation (12) yields equation (13):

$$T((k+1)T_0) = e^{-\frac{hA - I\frac{\partial V_{OCV}}{\partial T}}{mc}t}T(kT_0) + \frac{mc}{hA - I\frac{\partial V_{OCV}}{\partial T}}(1 - e^{-\frac{hA - I\frac{\partial V_{OCV}}{\partial T}}{mc}t}) \cdot (\frac{I^2R_r + hAT_\infty}{mc} + \frac{I_p^2R_p}{mc}) \quad (13)$$

The entropy coefficient of the battery is an important parameter for calculating the heat of reaction. The coefficient of entropy change is obtained from [33]. The temperature and the OCV are first-order fitted for a certain SOC. The slope of the first-order function is taken as the coefficient of entropy change. Figure 7 shows the entropy coefficient

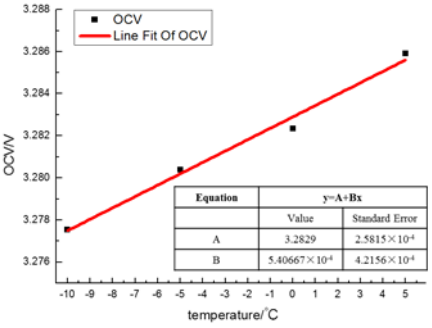

FIGURE 7. Entropy coefficient for SOC = 50%.

of SOC at 50%. The entropy change coefficients at different SOCs are calculated by using this method, and the entropy change coefficient curves for 10% SOC intervals are obtained as shown in Figure 8. The entropy change coefficient changes irregularly as SOC increases [34]. When the SOC is in the range of 10%∼90%, the entropy change coefficient is greater than zero. When the SOC is greater than 90%, the entropy change coefficient is less than zero. The value of the battery entropy change coefficient is small, which is always in the range of −0.2∼+1.8 mV/°C.

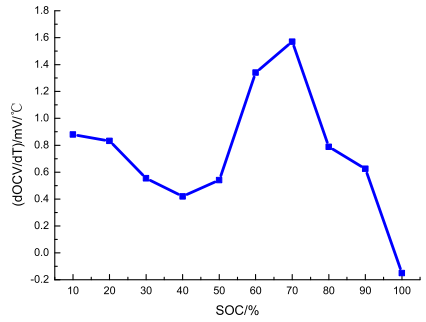

FIGURE 8. Entropy coefficient curve for different SOCs.

According to the reaction heat equation, a small entropy coefficient means that the reaction is a small part of the heat production. It also shows that the vast majority of heat is generated by Joule heating during battery discharge heating and that reaction heat does not contribute much to the battery temperature rise.

The battery heat dissipation during heating can be expressed by the equivalent heat transfer coefficient [35]. The equivalent heat transfer coefficient is an important parameter in the conservation of energy model, which can affect the accuracy of the battery temperature model [36]. An insulation film is attached around the battery for proper insulation during the experiment in order to reduce the battery heat convection in the heating process. When the battery is cooling at low temperatures, according to the law of conservation of energy, the battery equivalent heat transfer coefficient is shown as equation (14):

$$mc\frac{dT}{dt} = -hA(T - T_\infty) \quad (14)$$

Where, m = 145g, c = 1.13Jg^{-1} °C^{-1} [32], and T_∞ = −10 °C. Assuming that h is a constant, equation (14) can be expressed as equation (15):

$$\ln(T - T_\infty) = -\frac{hA}{mc}t + B \tag{15}$$

B can be obtained from the initial value. $\ln(T - T_\infty)$ is linear with t, and the equivalent heat transfer coefficient can be derived from the slope of the curve. The curves of T and $\ln(T - T_\infty)$ during battery cooling are shown in Figure 9. The relationship between $\ln(T - T_\infty)$ and $t$is approximately linear, and the result of equivalent thermal transfer coefficient h is 25.45 Wm^{-2}K^{-1}.

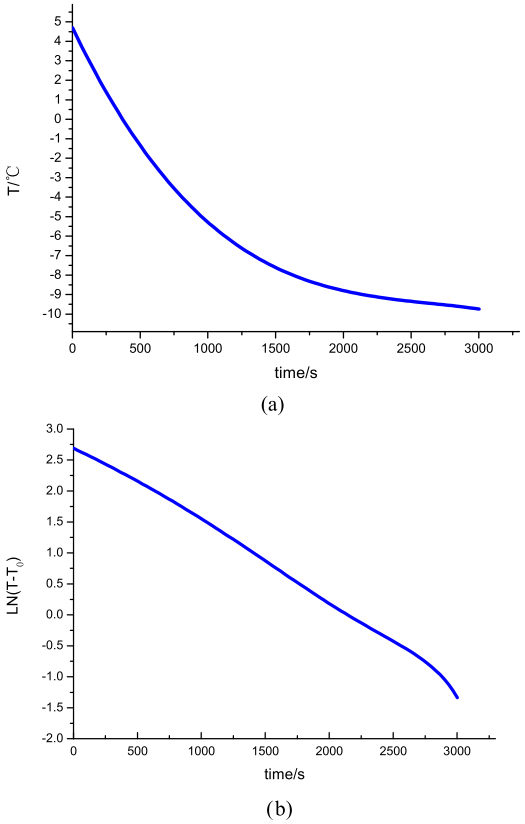

FIGURE 9. Curves of a) battery temperature and b) $\ln(T - T_\infty)$ when the battery cools down.

The entropy coefficient and the equivalent heat transfer coefficient are substituted into equation (13) to obtain the battery temperature-rise model. For the battery temperature model simulation and low temperature constant current discharge heating experiment, 2.4 C and 2.8 C are selected. The results of the simulation and experimental are shown in Figure 10. It can be seen from the figure that when the battery is heated by constant current discharge at different current magnifications, the simulation result of the battery temperature-rise model is substantially consistent with the actual temperature change of the battery, and the maximum error during the heating process does not exceed 1°C. It can be proven that the temperature-rise model established in this paper is valid and reliable.

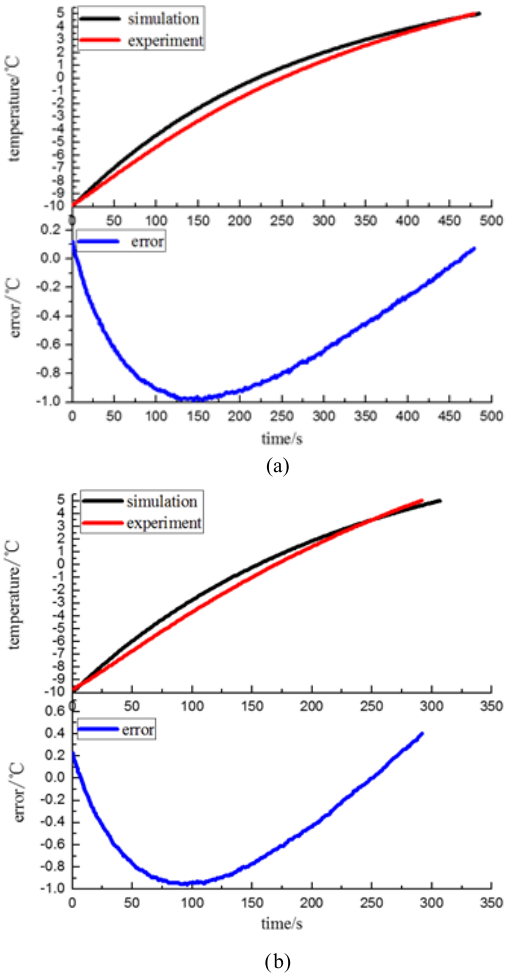

FIGURE 10. Comparison between the model estimated temperature curve and the actual temperature curve under different discharge currents heating at low temperatures. (a) Comparison between the model estimation temperature and actual measurement temperature of 12 A constant current discharge heating at low temperatures. (b) Comparison between the model estimation temperature and actual measurement temperature of 14 A constant current discharge heating at low temperatures.

III. MULTI-OBJECTIVE OPTIMIZATION OF DISCHARGE CURRENT FOR INTERNAL HEATING IN BATTERIES

The heating time and the capacity fade rate are important evaluation indexes of the heating method in the process of battery discharge for heating at low temperatures. However, there is a tradeoff between the capacity fade rate and the heating time in the heating process. How to choose an appropriate discharge current to weight these two factors is a key issue in the research of battery heating at low temperature.

A. THE DETERMINATION OF THE BOUNDARY CONDITIONS OF DISCHARGE CURRENT

According to the battery temperature-rise model established in this paper, the heat generated by the battery discharge should be greater than the heat dissipated to the outside world so that effective heating of the battery is achieved at low temperatures. Therefore, the determination of the boundary

conditions of discharge current is needed in applying the method of discharge for battery heating at low temperatures. The maximum discharge current during the progress of heating is the maximum discharge current (4 C) specified in the battery manual. The minimum discharge current should meet the requirement of equation (16):

$$I^2R_r + I_p^2R_p + IT\frac{\partial U_{OCV}}{\partial T} - hA(T - T_\infty) > 0 \quad (16)$$

Because the ohmic resistance and the polarization resistance of the battery are affected by the temperature and SOC, the minimum value of the discharge current gradually varies with the change of the battery temperature and SOC during heating process at low temperatures. The discharge current up boundary in the process of heating battery at an ambient temperature of −10°C is shown in Figure 11.

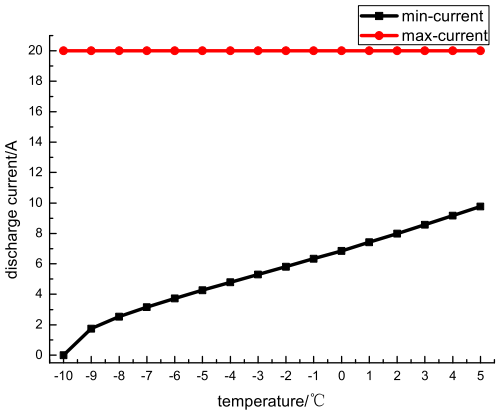

FIGURE 11. The boundary conditions of discharge current during battery heating.

It is found that the change of battery SOC during heating process at low temperatures is relatively small by our tests. Therefore we can ignore its effect of temperature on the boundary conditions of the discharge current. As a result, the minimum value of discharging current only varies with temperature.

B. ESTABLISHMENT OF AN OPTIMIZING OBJECTIVE FUNCTION

The battery capacity depreciation model is important to realize the optimal objective. The battery degradation is influenced by temperature, charge/discharge rate, internal resistance and SOC greatly. In this research, the battery degradation model [37] is shown in equation (17).

$$Q_{loss} = 0.0032e^{-\left(\frac{15162-1516C\_Rate}{R(|285.75-T_{bat}|+265)}\right)}(A_h)^{0.849} \quad (17)$$

where, Q_{loss} is the percentage of capacity loss; C_Rate is current rate; R is the gas constant; T_{bat} is the battery temperature; A_h is ampere-hour throughput.

The parameters for battery degradation model for $LiFePO_4$ is obtained from charge/discharge testing cycles by alternating constant current experiments under 5°C and 45°C respectively. Due to the limit of maximum discharge current capability for thermal chamber, the maximum discharge rate for the selected battery can only be set as 3 C. The battery capacity fade is primarily the result of loss of active lithium associated with anode degradation [38], therefore, the battery degradation model would be suitable for higher current rate with acceptable errors and no lithium deposition, if the battery has the same material and the discharge current doesn't cause lithium precipitation. The 4 C is not enough to induce lithium deposition, therefore, the battery degradation model can be used normally in the temperature range of −20°C∼+10°C and when the discharge current rate is in the range of 0.5 C∼4 C.

To construct the optimization objective function, the heating process is first divided into N phases, every 1°C rise of the battery is denoted as a heating phase, and the parameters of the battery degradation model are considered constant in each heating phase. According to the temperature-rise model established in this paper, with $\Delta T = 1$ in equation (9), the time required for the ***j***th heating phase is

$$t_j = \frac{mc}{\left(I_j\frac{\partial V_{OCV}}{\partial T} - hA\right)T(j) + I_j^2R_{r,j} + I_{p,j}^2R_p + hAT_\infty}$$
$$j = 1, 2, 3\cdots N \quad (18)$$

Ampere-hour integral estimation has a very low computational complexity and is widely used [39]. The change of SOC in the ***j***th heating phase is

$$\Delta SOC = \frac{\int_0^{t_j} I_j dt}{3600Cap} \quad (19)$$

Where, Cap is the rated capacity of the battery, and the unit is Ah.

When the sampling time of the battery management system is Δt, the number of samples in each heating phase is

$$M_j = \frac{t_j}{\Delta t} \quad (20)$$

Since $A_h = I \cdot t$, substituting equation (18) into equation (17) gives the capacity fade of the jth heating phase as

$$Q_{loss,j} = 0.0032e^{-\left(\frac{15162-1516C\_Rate}{R(|285.75-T_{bat}|+265)}\right)}(I_j \cdot D_1)^{0.849} \quad (21)$$

$$D_1 = \frac{mc}{\left(I_j\frac{\partial V_{OCV}}{\partial T} - hA\right)T(j) + I_j^2R_{r,j} + I_{p,j}^2R_p + hAT_\infty} \quad (22)$$

where, Q_{loss} is the percentage of capacity loss; C_Rate is the battery discharge rate, R is the ideal gas constant, A is the surface area of the battery, I_j is the discharge current for the ***j***th heating phase, T (j) is the battery temperature in the ***j***th phase, and $R_{r,j}$ and $R_{p,j}$, respectively, correspond to the ohmic resistance and polarization resistance for the ***j***th heating phase, which are affected by the current battery temperature and SOC. t_j is the time of the ***j***th heating phase, and $I_{p,j,k}$ is the current of the ***k***th sampling time of the polarization

resistor $R_{p,j}(I_j)$ in the jth heating phase, which can be obtained by the full response formula of the first-order RC circuit:

$$\mathrm{I_{p,j,k}} = \mathrm{I_j}(1 - \mathrm{e}^{-\frac{k\Delta t}{R_{p,j}C_{p,j}}}) + \frac{\mathrm{U_{p,j}}}{\mathrm{R_{p,j}(I_j)}}\mathrm{e}^{-\frac{k\Delta t}{R_{p,j}C_{p,j}}} \tag{23}$$

Where, $\mathrm{U_{p,j}}$ is the polarization voltage at the start of the jth discharge heating process.

The discretization of formula (21) can be expressed (24) and (25), as shown at the bottom of this page.

The battery capacity fade in the entire heating process is

$$Q_{loss} = \sum_{j=1}^{N}\sum_{k=1}^{M_j} 0.0032e^{-\left(\frac{15162-1516C\_Rate}{R(|285.75-T_{bat}|+265)}\right)}(I_j \cdot D_3)^{0.849} \tag{26}$$

Where (27), as shown at the bottom of this page.

The total time of the entire heating process is (28), as shown at the bottom of this page.

The battery capacity degradation and heating time do not have the same order of magnitude. To make the optimization objective function contain both variables, the paper normalizes the battery capacity fade and heating time by min-max standardization, and the original data are linearly converted so that the result value is mapped to [0-1]. The conversion function is shown in equation (29):

$$x^* = \frac{x - \min}{\max - \min} \tag{29}$$

Where, ***max*** is the maximum sample data, and ***min*** is the minimum sample data.

Refer to [40], the trade-off between capacity degradation and heating time may be captured by the use of a weight factor. When $\Delta t = 1$ is set as the system sampling time, the objective function of the optimization heating method proposed in this paper can be expressed as

$$f = \min\left\{\alpha\sum_{j=1}^{N} Q^*_{loss,j} + (1-\alpha)\sum_{j=1}^{N} t^*_j\right\} \tag{30}$$

Where, α is the weight factor, and $Q^*_{loss,j}$ and t^*_j are the battery capacity fade and heating time after the standardization, respectively.

In this paper, the polarization resistance and capacitance are parallel in the Thevenin equivalent circuit model, meaning that the pressure drop of the polarization resistance cannot be abrupt. Therefore, the initial polarization voltage of each discharge heating phase is equal to the termination polarization voltage corresponding to the previous discharge heating phase. The initial polarization voltage of each heating phase is set as the state variable in this paper, and the state transition equation is

$$[\mathrm{I_j}(1 - \mathrm{e}^{-\frac{36C/\mathrm{I_j}}{R_{p,j}(I_j)C_{p,j}(I_j)}}) + \frac{\mathrm{U_{p,j}}}{\mathrm{R_{p,j}(I_j)}}\mathrm{e}^{-\frac{36C/\mathrm{I_j}}{R_{p,j}(I_j)C_{p,j}(I_j)}}]\mathrm{R_{p,j}(I_j)} = \mathrm{U_{1(j+1)}} \quad \mathrm{j} = 1, 2 \ldots \mathrm{N}-1 \tag{31}$$

At the end of the discharge heating process, the current in the polarization resistor is considered to have reached a steady state current, which is I_N. The polarization voltage at the beginning of the last heating phase can be obtained from equation (31), which is the state variables $U_{P,N} = I_N R_{p,N}$. At the start of discharge heating, since the voltage across the polarization resistor is zero, the state variable $U_{p,1}$ of this heating phase is zero.

C. USING THE DYNAMIC PROGRAMMING ALGORITHM TO OBTAIN THE DISCHARGE CURRENT

The dynamic programming (DP) algorithm is one of the most effective mathematical methods to solve the global optimization problem. It can be applied in the multi-objective optimization system of discharging for internal heating of lithium-ion batteries and the optimal control strategy of discharging current for heating. The dynamic programming strategy for optimal heating discharge current involves much calculation so that it is difficult to utilize in online applications and other areas. However, the global optimal solution obtained through offline optimization can determine the limit of the target function range, which is of great value to other current control strategy evaluations. Therefore, the dynamic programming algorithm is widely used in offline global optimization of nonlinear systems.

The dynamic programming algorithm (DP) is used to solve the function of the proposed electric heating method in this paper.

$$Q_{loss,j} = \sum_{k=1}^{M_j} 0.0032e^{-\left(\frac{15162-1516C\_Rate}{R(|285.75-T_{bat}|+265)}\right)}(I_j \cdot D_2)^{0.849} \tag{24}$$

$$D_2 = \frac{mc}{\left(I_j\frac{\partial V_{OCV}}{\partial T} - hA\right)T(j) + I_j^2R_{r,j} + I_j(1 - e^{-\frac{k\Delta t}{R_{p,j}C_{p,j}}}) + \frac{U_{p,j}}{R_{p,j}(I_j)}e^{-\frac{k\Delta t}{R_{p,j}C_{p,j}}} + hAT_\infty} \tag{25}$$

$$D_3 = \frac{mc}{\left(I_j\frac{\partial V_{OCV}}{\partial T} - hA\right)T(j) + I_j^2R_{r,j} + I_j(1 - e^{-\frac{k\Delta t}{R_{p,j}C_{p,j}}}) + \frac{U_{p,j}}{R_{p,j}(I_j)}e^{-\frac{k\Delta t}{R_{p,j}C_{p,j}}} + hAT_\infty} \tag{27}$$

$$t = \sum_{j=1}^{N}\sum_{k=1}^{M_j} \frac{mc}{\left(I_j\frac{\partial V_{OCV}}{\partial T} - hA\right)T(j) + I_j^2R_{r,j} + I_j(1 - e^{-\frac{k\Delta t}{R_{p,j}C_{p,j}}}) + \frac{U_{p,j}}{R_{p,j}(I_j)}e^{-\frac{k\Delta t}{R_{p,j}C_{p,j}}} + hAT_\infty} \tag{28}$$

The stage variable is the heating phase, which is divided by the change of the battery temperature. Each heating phase is denoted by j, $j = 1, 2, \ldots N$.

The state variable $U_{p,j}$ is the polarization voltage at the start of the jth heating phase.

The decision variable I_j is the discharge current in the ***j***th heating phase.

The allowed decision set is shown in equation (32):

$$D_j(I_j) = \{I_{min} \le I_j \le I_{max}\} \tag{32}$$

The state transition equation is shown in equation (33):

$$\begin{cases} U_{p,j+1} = \Phi(U_{p,j}, I_j)[I_j(1 - e^{-\frac{36Cap/I_j}{R_{p,j}C_{p,j}}}) + \frac{U_{p,j}}{R_{p,j}} e^{-\frac{36Cap/I_j}{R_{p,j}C_{p,j}}}]R_{p,j}(I_j) \\ j = 1, 2 \ldots N - 1 \\ U_{p,N} = R_{p,N} I_N \\ U_{p,1} = 0 \end{cases} \tag{33}$$

The compensation function selects the weighted sum of the battery capacity fade and heating time after normalization in the ***j***th heating phase as

$$V_j = \alpha Q^*_{loss,j} + (1 - \alpha) t^*_j \tag{34}$$

The target optimal value function f_j represents the minimum of the weighted sum of the battery capacity fade and heating time from the ***j***th to the ***N***th heating phases.

$$f_j = \min \left\{ \alpha \sum_{j=1}^{N} Q^*_{loss,j} + (1 - \alpha) \sum_{j=1}^{N} t^*_j \right\} \tag{35}$$

The ***N***th heating phase is increased from the initial stage when applying the dynamic programming algorithm, and the optimal objective function of this phase is set as zero, which is $f_{N+1} = 0$.

Therefore, the DP model of the heating optimization problem is

$$\begin{cases} f_j(U_{p,j}) = \min\limits_{I_j \in D_j(I_j)} [v_j(U_{p,j}) + f_{j+1}(U_{j+1})] \\ j = N, N - 1, \ldots 1 \\ f_{N+1} = 0 \end{cases} \tag{36}$$

The progress of using the dynamic programming algorithm to solve the current is shown in Figure 12. The inverse method is used in the calculation process.

First, the extreme value of f_N is obtained, and the optimal discharge current in the Nth stage is obtained, which is $I_{N,opt} = M_N(U_{1,N})$. Substituting $U_{p,N}$ and $I_{N,opt}$ into f_N gives the expression f_N for $U_{p,N}$, which is $P_N(U_{p,N})$. According to the state transfer equation, $P_N(U_{p,N})$ is further expressed as $P_N(\varphi(U_{p,N-1}, I_{N-1}))$. After storing $I_{N,opt}$ and f_N, f_{N-1} is calculated by the same method to obtain $I_{N-1,opt}$ and f_{N-1}, which are further expressed as $M_{N-1}(U_{p,N-1,opt})$ and $P_{N-1}(\varphi(U_{p,N-2}, I_{N-2}))$. After storing $I_{N-1,opt}$ and f_{N-1}, f_{N-2} is calculated. Through such forward projections, each phase discharge current $I_{j,opt}$ can be expressed as a function of $U_{p,j}$ in the form $M_j(U_{p,j})$. According to the initial condition,

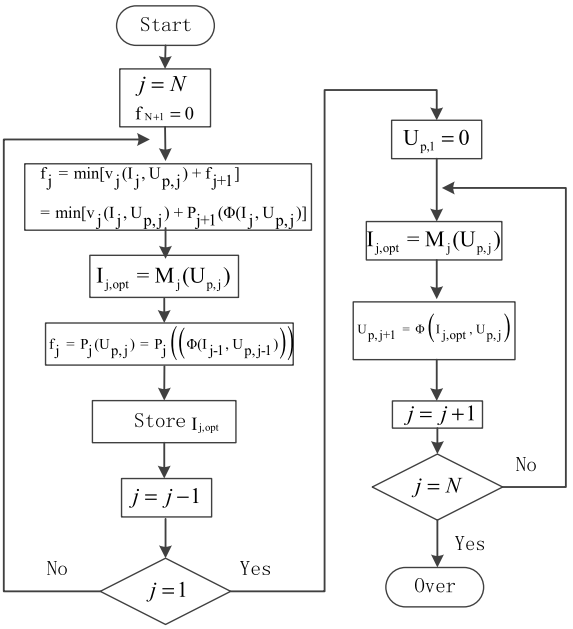

FIGURE 12. Flow chart of the dynamic programming algorithm to solve for current.

which is $U_{p,1} = 0$, and the state transition equation, which is $U_{p,j} = \varphi(U_{p,j-1}, I_{j-1})$, the optimal discharge current of each stage, I_j., is obtained by calculating from front to back.

IV. SIMULATION AND EXPERIMENTAL RESULT ANALYSIS

A. THE RESULTS OF THE DISCHARGE HEATING OPTIMIZATION METHOD

Considering the polarization resistance between 90%∼100% SOC is significant high, therefore the initial SOC is set as 90% for heating process. For the weighting factor of the optimization goal changing from 0 to 1, the optimization results of the proposed electric heating method are shown in Figure 13. The temperature range of battery heating is −10°C∼+5°C. As seen from Figure 11, when the weight factor is 0, the optimal discharge current obtained by the multi-objective optimization heating method is a constant value (20 A), which is the maximum value of the discharge current

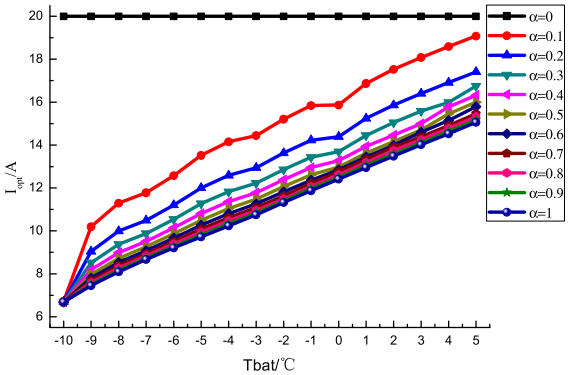

FIGURE 13. The discharging current for different weight factors.

boundary condition. The weight factor is 0, this means that the influence of the battery heating process on the capacity fade can be completely ignored. The heating time is reduced as much as possible so that the discharge current remains at a maximum. When the weighting factor is greater than 0, the initial discharge current at the beginning of battery heating at low temperatures is 6.7 A. The optimal heating discharge current gradually increases on this basis with the gradual increase of the battery temperature during heating. The optimal discharge heating current will increase to 15.06∼19.08 A when the battery reaches the target temperature of 5 °C.

The optimal discharge currents obtained under different weighting factors were used to simulate the battery heating at low temperatures, and the heating time and capacity fade under different weighting factors were obtained as shown in Figure 14. As shown in Figure 14, regardless of what the weight factor value is, the amount of battery capacity fade caused by each low-temperature heating process is 10^{-5}Ah. The heating time increases with the increase of the weighting factor, while the capacity fade decreases with the increase of the weighting factor as an overall trend. This further shows that the heating time and capacity fade during battery low-temperature discharge heating have an inverse relationship. When the weighting factor is increased from 0 to 0.1, the heating time and the capacity fade are greatly changed. With the gradual increase of the weighting factor, the change of the heating effect caused by each change of 0.1 gradually decreases. When the weighting factor continues to increase from 0.5, the increase of the heating time and the decline of the capacity fade are obviously slowed down.

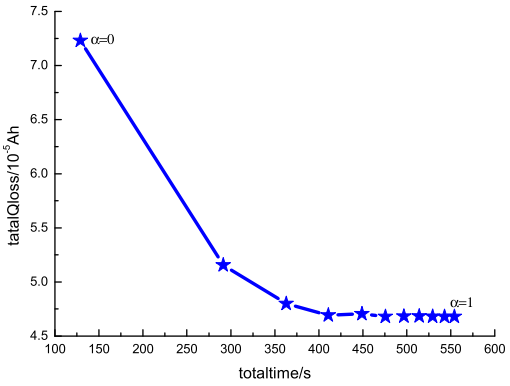

FIGURE 14. The capacity fade in heating process for different weight factors.

In addition, as seen from Figure 12, the curve has a small fluctuation in the range of the weighting factor from 0.3 to 0.4. When the weight factor is 0.4, the heating time and capacity attenuation values are greater than those for the weight value of 0.3. This is due to the non-linear relationship between the battery internal and external parameters (including temperature and SOC).

Figure 15 shows the curves of the prediction by the battery model, the curves of the actual temperature and the error curve between the above two when the weighting factors are

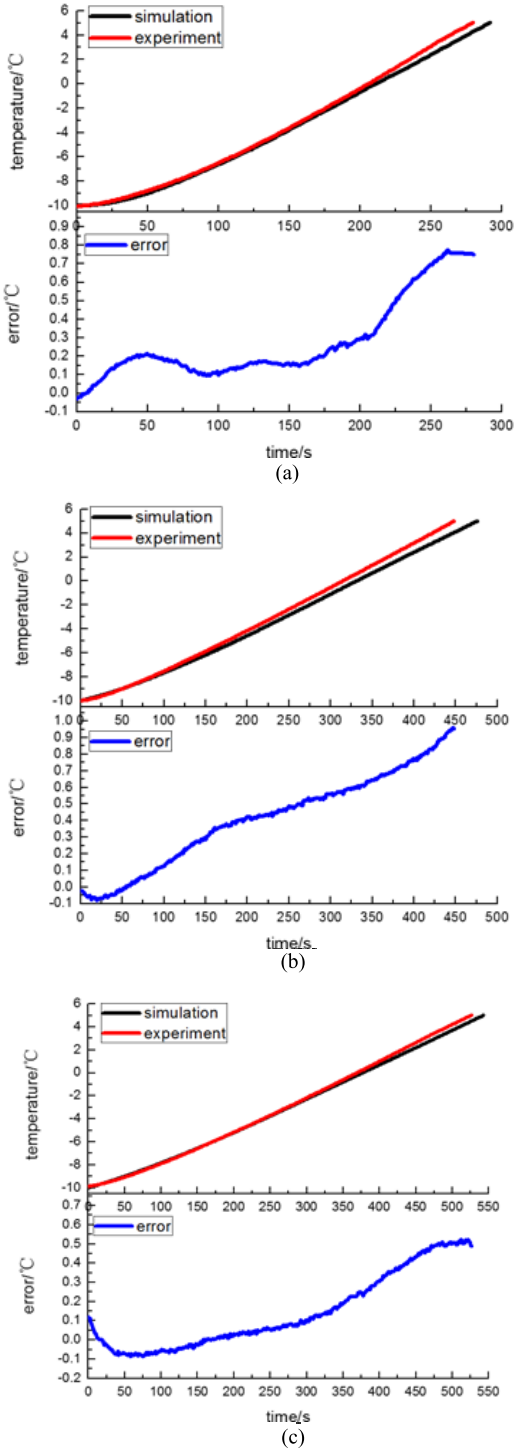

FIGURE 15. Comparison of the temperature predicted by battery model with the temperature measured in the test when the weight factor is a) 0.1, b) 0.5 and c) 0.9.

0.1, 0.5 and 0.9. In the process of heating the battery temperature from −10°C to 5°C, the error between the predicted temperature of the battery model and the actual measured temperature of the battery is controlled within 1°C. It can be proved that the battery temperature-rise model established in this paper is valid

B. THE RESULTS OF THE CONSTANT-CURRENT DISCHARGING METHOD

The capacity degradation and energy consumption during the heating process varies at the different discharge rate. Therefore, they are selected as decision variables to find the optimal value of constant current discharge rate. Figure 16 shows the capacity degradation and energy consumption for different discharge rate in the range of 2C∼4C. The capacity fade is minimum at the discharge rate of 2.4C (12A), and the power consumption is at flat low value area. Therefore, 2.4C is an optimal discharge rate value for constant discharge method to compare its performance with that of optimal discharge strategy.

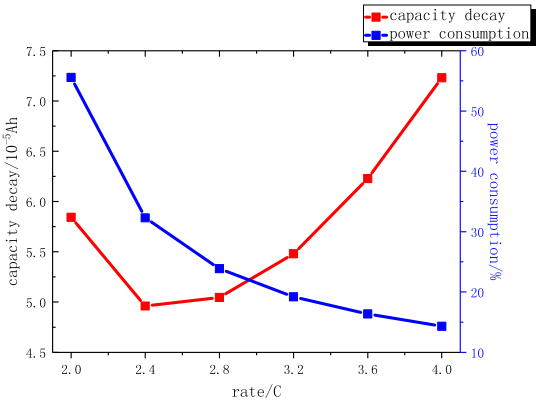

FIGURE 16. The performance capacity degradation and energy consumption at different discharge rates.

C. ANALYSIS OF THE WEIGHT FACTOR

To verify the effectiveness of the proposed heating method and provided a reference for choosing a reasonable weight factor, it is compared with the constant current discharge heating method by a 2.4 C discharge rate. The range of the weight factor for the proposed method covers 0.1∼0.9, and the discharge current is set as12 A for the constant current discharge heating method based on the analysis in former section. The battery capacity fade by two methods after the heating process are compared shown as Table 3.

From the results in TABLE 3, the degradation may be looks not obvious especially when the weight factor is larger than 0.5 in only limited discharge cycles, however, in practical applications, the capacity degradation difference influenced by various discharge method will be significant by amounts cycles after long-term use.

To compare the effectiveness of the two kinds of heating methods, the evaluating indicator is proposed as follows:

$$\gamma_{\alpha,\mathrm{Qloss}} = \frac{\mathrm{Qloss_{cc}} - \mathrm{Qloss}_{\alpha}}{\mathrm{Qloss_{cc}}} \times 100\% \tag{37}$$

$$\gamma_{\alpha,\mathrm{t}} = \frac{\mathrm{t_{cc}} - \mathrm{t}_{\alpha}}{\mathrm{t_{cc}}} \times 100\% \tag{38}$$

In equations (37) and (38), $\gamma_{\alpha,Qloss}$ and $\gamma_{\alpha,t}$, respectively, represent the percentage of savings in the capacity fade and heating time of the optimized heating method relative to the constant current discharge heating method. Qloss_{α} and t_{α}, respectively, represent the capacity fade and heating time corresponding to the weight factor $\propto$. Qloss_{cc} and t_{cc}, respectively, represent the capacity fade and heating time of the 12 A constant current discharge heating method. The result of the comparison is shown in Figure 17.

TABLE 3. The capacity fade comparison between the optimal and constant-current discharging heating method.

Heating method			Capacity fade (10^{-5} Ah)	Heating time (s)
Heating method proposed in the paper	weight factor	0.1	5.1564	291.33
		0.2	4.8002	362.78
		0.3	4.6924	410.74
		0.4	4.7052	449.02
		0.5	4.6796	475.54
		0.6	4.6835	496.64
		0.7	4.6850	514.07
		0.8	4.6808	529.31
		0.9	4.6800	542.83
12 A constant-current discharging method			4.9599	484.31

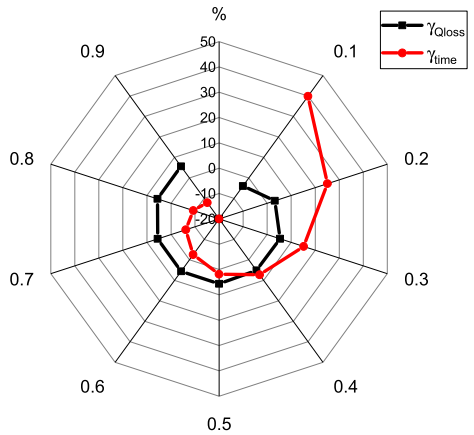

FIGURE 17. Comparison of multi-objective optimization for heating batteries at different weight factors and constant current discharge battery heating.

As seen from Figure 17, the heating time required for the heating method proposed in this paper is basically the same as that of the 12 A constant current discharge method when the weight factor is 0.5. However, the capacity fade of the heating method proposed in this paper is 5.65% less than that of the constant current heating method. When the weight factor is less than 0.5, the heating time of the heating method proposed in this paper is 7.28%∼39.85% less than that of the constant current heating method. In addition, when the weight factor is greater than 0.1, the capacity fade of the heating method proposed in this paper is 3.22%∼5.64% less than that of the constant current heating method. According to the optimized heating method proposed in this paper, the discharge current varies with the change of the internal

parameters of the battery, which is caused by the change of SOC. Therefore, the battery heating method proposed in this paper not only helps to reduce the capacity fade of the battery but also achieves the purpose of balancing the capacity fade and heating time.

D. COMPARISON OF POWER CONSUMPTION

To further illustrate the advantages of the proposed optimization methods, this paper compares the heating method and the constant current discharge heating method based on the power consumption. In this research, the power consumption refers to the power consumption during the heating process. For convenient, changing rate of SOC in the heating phase is adopted to characterize it as shown in equation (19).

$$\Delta SOC = \sum_{j=1}^{N} \frac{\int_0^{t_j} I_j dt}{3600 Cap} \tag{39}$$

The power consumption of the optimization heating method corresponding to different weighting factors are compared with that of the 12 A constant current discharge heating method. The comparison result is shown in Figure 18.

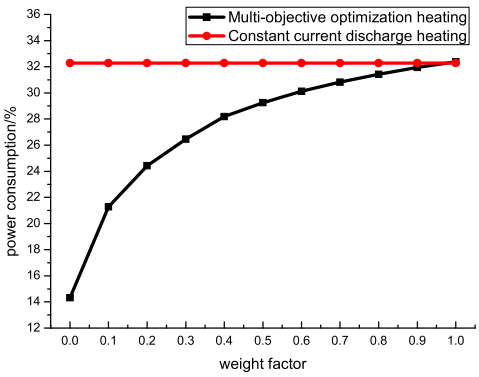

FIGURE 18. Power consumption of two heating methods during the heating process.

As seen from Figure 18, the power consumption in the heating process gradually increases with the weighting factor. When the weighting factor is increased to the range of 0.9∼1, the power consumption of the method proposed in this paper is the same as that of the constant current discharge heating method whose current value is 12 A, and the value of the power consumption is 32.82%. In addition, when the weighting factor is 0.5, the power consumption of the optimization heating method in the heating progress is 29.24%, which is obviously smaller than that of the constant current discharge heating method. To sum up, compared with the constant current discharge heating method, when the weighting factor is 0.5, the corresponding capacity fade decreases by 5.65%, the heating time decreases by 1.82% and the power consumption decreases by 3.04%. Therefore, the optimization heating method proposed in this paper can effectively reduce the capacity fade and the power consumption without increasing the heating time.

V. CONCLUSION

Based on the Thevenin equivalent circuit model and the battery temperature-rise model, combined with parameter recognition, a self-heating method is proposed. The method takes the capacity fade rate and heating time as the optimization target, and the DP algorithm as global optimization strategy to obtain the optimal current curve.

The results of the simulations and experiments show that the optimal discharge strategy have different emphasis on the capacity fade and heating time during different heating stages. For example, in the process of the battery temperature being increased from −10°C to +5°C, compared with the constant current discharge method, both the capacity fade and power consumption are all decreased, however the heating time has no significant increasing with 0.5 weighting factor. By the experiment results, it can be found that the capacity fade is decreased by 5.65%, the heating time decreased by 1.82%, and the power consumption decreased by 3.04%. However, if the weight factor is less than 0.5, the heating time of the optimization heating method is less than that of the constant current discharge heating method by a decreasing from 7.28% to 39.85%. Otherwise, if the weight factor is greater than 0.1, the capacity fade of the optimization heating method is less than that of the constant current discharge heating method by a reduction from 3.22% to 5.64%. Therefore, the optimal self-heating method proposed in this paper can improve the heating efficiency and reduce heating time, with minimum batter capacity fade under low temperature by changing the weight factor.

REFERENCES

[1] F. Sun, R. Xiong, and H. He, "A systematic state-of-charge estimation framework for multi-cell battery pack in electric vehicles using bias correction technique," *Apply Energy*, vol. 162, pp. 1399–1409, Jan. 2016.
[2] T. M. Bandhauer, S. Garimella, and T. F. Fuller, "A critical review of thermal issues in lithium-ion batteries," *J. Electrochem. Soc.*, vol. 158, no. 3, pp. R1–R25, 2011.
[3] L. Zhe, H. Xuebing, L. Lu, and M. Ouyang, "Temperature characteristics of power $LiFePO_4$ batteries," *J. Mech. Eng.*, vol. 47, no. 18, pp. 115–120, 2011.
[4] A. Senyshyn, M. J. Mühlbauer, O. Dolotko, and H. Ehrenberg, "Low-temperature performance of Li-ion batteries: The behavior of lithiated graphite," *J. Power Sources*, vol. 282, pp. 235–240, May 2015.
[5] S. Tippmann, D. Walper, L. Balboa, B. Spier, and W. G. Bessler, "Low-temperature charging of lithium-ion cells part I: Electrochemical modeling and experimental investigation of degradation behavior," *J. Power Sources*, vol. 252, pp. 305–316, Apr. 2014.
[6] J. Jaguemont, L. Boulon, and Y. Dubé, "A comprehensive review of lithium-ion batteries used in hybrid and electric vehicles at cold temperatures," *Appl. Energy*, vol. 164, pp. 99–114, Feb. 2016.
[7] J. Jaguemont, L. Boulon, and Y. Dubé, "Characterization and modeling of a hybrid-electric-vehicle lithium-ion battery pack at low temperatures," *IEEE Trans. Veh. Technol.*, vol. 65, no. 1, pp. 1–14, Jan. 2015.
[8] M. A. Hannan, F. A. Azidin, and A. Mohamed, "Hybrid electric vehicles and their challenges: A review," *Renew. Sustain. Energy Rev.*, vol. 29, pp. 135–150, Jan. 2014.
[9] Z. Lei, C. Zhang, J. Li, G. Fan, and Z. Lin, "Preheating method of lithium-ion batteries in an electric vehicle," *J. Mod. Power Syst. Clean Energy*, vol. 3, no. 2, pp. 289–296, 2015.

[10] H.-S. Song *et al.*, "Experimental study on the effects of pre-heating a battery in a low-temperature environment," in *Proc. Vehicle Power Propuls. Conf.*, Oct. 2012, pp. 1198–1201.
[11] T. Zhu *et al.*, "An optimized energy management strategy for preheating vehicle-mounted Li-ion batteries at subzero temperatures," *Energies*, vol. 10, no. 2, p. 243, 2017.
[12] C.-N. Zhang, Z.-G. Lei, and Y.-G. Dong, "Method for heating low-temperature lithium battery in electric vehicle," *Trans. Beijing Inst. Technol.*, vol. 32, no. 9, pp. 921–925, 2012.
[13] K. Murashko *et al.*, "Modelling of the battery pack thermal management system for hybrid electric vehicles," in *Proc. IEEE Eur. Conf. Power Electron. Appl.*, Aug. 2014, pp. 1–10.
[14] R. Xiong, F. Sun, Z. Chen, and H. He, "A data-driven multi-scale extended Kalman filtering based parameter and state estimation approach of lithium-ion olymer battery in electric vehicles," *Appl. Energy*, vol. 113, no. 1, pp. 463–476, 2014.
[15] Y. Ji and C. Y. Wang, "Heating strategies for Li-ion batteries operated from subzero temperatures," *Electrochimica Acta*, vol. 107, pp. 664–674, Sep. 2013.
[16] J. Zhang, H. Ge, Z. Li, and Z. Ding, "Internal heating of lithium-ion batteries using alternating current based on the heat generation model in frequency domain," *J. Power Sources*, vol. 273, pp. 1030–1037, Jan. 2015.
[17] S. Mohany, Y. Kim, A. G. Stefanopoulou, and Y. Ding, "On the warmup of Li-ion cells from sub-zero temperatures," in *Proc. Amer. Control Conf.*, 2014, pp. 1547–1552.
[18] X. W. Zhao, G. Y. Zhang, L. Yang, J. X. Qiang, and Z. Q. Chen, "A new charging mode of Li-ion batteries with $LiFePO_4$/C composites under low temperature," *J. Thermal Anal. Calorimetry*, vol. 104, no. 2, pp. 561–567, 2011.
[19] H. Ruan *et al.*, "A rapid low-temperature internal heating strategy with optimal frequency based on constant polarization voltage for lithium-ion batteries," *Appl. Energy*, vol. 177, pp. 771–782, Sep. 2016.
[20] G. Zhang, S. Ge, T. Xu, X.-G. Yang, H. Tian, and C.-Y. Wang, "Rapid self-heating and internal temperature sensing of lithium-ion batteries at low temperatures," *Electrochimica Acta*, vol. 218, pp. 149–155, Nov. 2016.
[21] J. Sun *et al.*, "Low current rate discharge with external heating at low temperature," in *Proc. VPPC*, 2015, pp. 1–5.
[22] C. Wang, T. Xu, S. Ge, G. Zhang, X. Yang, and Y. Ji, "A fast rechargeable lithium-ion battery at subfreezing," *J. Electrochem. Soc.*, vol. 163, no. 9, pp. A1944–A1950, 2016.
[23] C. Zhang, X. Jin, and J. Li, "PTC self-heating experiments and thermal modeling of lithium-ion battery pack in electric vehicles," *Energies*, vol. 10, no. 4, p. 572, 2017.
[24] M. Ouyang *et al.*, "Low temperature aging mechanism identification and lithium deposition in a large format lithium iron phosphate battery for different charge profiles," *J. Power Sources*, vol. 286, pp. 309–320, Jul. 2015.
[25] K. Jalkanen, J. Karppinen, L. Skogström, T. Laurila, M. Nisula, and K. Vuorilehto, "Cycle aging of commercial NMC/graphite pouch cells at different temperatures," *Appl. Energy*, vol. 154, pp. 160–172, Sep. 2015.
[26] X. Hu, C. Zou, C. Zhang, and Y. Li, "Technological developments in batteries: A survey of principal roles, types, and management needs," *IEEE Power Energy Mag.*, vol. 15, no. 5, pp. 20–31, Sep./Oct. 2017.
[27] X. Wu, Z. Mei, C. Hu, C. Zhu, and J. Sun, "Temperature performance comparative analysis of different power batteries," in *Proc. IEEE Vehicle Power Propuls. Conf.*, Oct. 2016, pp. 1–6.
[28] T. Zahid and W. Li, "A comparative study based on the least square parameter identification method for state of charge estimation of a $LiFePO_4$ battery pack using three model-based algorithms forelectric vehicles," *Energies*, vol. 9, no. 9, p. 720, 2016.
[29] G. Liu, M. Ouyang, L. Lu, J. Li, and X. Han, "Analysis of the heat generation of lithium-ion battery during charging and discharging considering different influencing factors," *J. Thermal Anal. Calorimetry*, vol. 116, no. 2, pp. 1001–1010, 2014.
[30] V. V. Viswanathan *et al.*, "Effect of entropy change of lithium intercalation in cathodes and anodes on Li-ion battery thermal management," *J. Power Sources*, vol. 195, no. 11, pp. 3720–3729, 2010.
[31] Y. Zhang, R. Xiong, H. He, and W. Shen, "Lithium-ion battery pack state of charge and state of energy estimation algorithms using a hardware-in-the-loop validation," *IEEE Trans. Power Electron.*, vol. 32, no. 6, pp. 4421–4431, Jun. 2017.
[32] X. Wu, Z. Chen, and Z. Wang, "Analysis of low temperature preheating effect based on battery temperature-rise model," *Energies*, vol. 10, no. 8, p. 1121, 2017.
[33] H. Ruan, J. Jiang, B. Sun, N. Wu, W. Shi, and Y. Zhang, "Stepwise segmented charging technique for lithium-ion battery to induce thermal management by low-temperature internal heating," in *Proc. IEEE Transport. Electrific. Asia–Pacific*, Aug./Sep. 2014, pp. 1–6.
[34] J. Sun *et al.*, "Online internal temperature estimation for lithium-ion batteries based on Kalman filter," *Energies*, vol. 8, no. 5, pp. 4400–4415, 2015.
[35] H. Ge, J. Huang, J. Zhang, and Z. Li, "Temperature-adaptive alternating current preheating of lithium-ion batteries with lithium deposition prevention," *J. Electrochem. Soc.*, vol. 163, no. 2, pp. A290–A299, 2016.
[36] J. Sun *et al.*, "The method of online temperature estimation for electric vehicle battery," *Trans. China Electrotech. Soc.*, vol. 32, no. 7, pp. 197–203, 2017.
[37] Z. Song, H. Hofmann, J. Li, J. Hou, X. Zhang, and M. Ouyang, "The optimization of a hybrid energy storage system at subzero temperatures: Energy management strategy design and battery heating requirement analysis," *Appl. Energy*, vol. 159, pp. 576–588, Dec. 2015.
[38] J. Wang *et al.*, "Cycle-life model for graphite-$LiFePO_4$ cells," *J. Power Sources*, vol. 196, no. 8, pp. 3942–3948, 2011.
[39] Y. Zheng, M. Ouyang, X. Han, L. Lu, and J. Li, "investigating the error sources of the online state of charge estimation methods for lithium-ion batteries in electric vehicles," *J. Power Sources*, vol. 377, pp. 161–188, Feb. 2018.
[40] C. Zou, X. Hu, Z. Wei, and X. Tang, "Electrothermal dynamics-conscious lithium-ion battery cell-level charging management via state-monitored predictive control," *Energy*, vol. 141, pp. 250–259, Dec. 2017.

JIUYU DU received the Ph.D. degree from the Beijing Institute of Technology in 2009. She is currently an Assistant Professor of the Department of Automotive Engineering, Tsinghua University. Her research mainly focuses on battery safety, durability issues and electrical & thermal management systems for electric vehicle and energy storage grid.

ZHE CHEN received the master's degree in electrical engineering with the Harbin University of Science and Technology. He studied in the Department of Automotive Engineering, Tsinghua University, from 2017 to 2018. His research mainly focuses on the battery management systems for electric vehicles.

FEIQIANG LI received the Ph.D. degree from the Beijing Institute of Technology in 2010. He is currently a Post-Doctoral Fellow with the Department of Automotive Engineering, Tsinghua University. His research mainly focuses on electric vehicle safety and control.